Journal of Sound and Vibration (2002) **252**(1), 1–17
doi:10.1006/jsvi.2001.4020, available online at http://www.idealibrary.com on IDEAL®

TRANSIENT ANALYSIS OF RING-STIFFENED COMPOSITE CYLINDRICAL SHELLS WITH BOTH EDGES CLAMPED

Y.-W. KIM

Department of Mechanical Engineering, Yosu National University, Yosu, Chonnam 550-749, *Korea.*
E-mail: ywkim@yosu.ac.kr

AND

Y.-S. LEE

Department of Mechanical Design Engineering, Chungnam National University, Taejon 305-764, *Korea*

(*Received* 18 *May* 2001, *and in final form* 11 *September* 2001)

A theoretical method is developed to investigate the effects of ring stiffeners on vibration characteristics and transient responses for the ring-stiffened composite cylindrical shells subjected to the step pulse loading. Love's thin shell theory combined with the discrete stiffener theory to consider the ring stiffening effect is adopted to formulate the theoretical model. The ring stiffeners are laminated with a composite material and have a uniform rectangular cross-section. The Rayleigh–Ritz procedure is applied to obtain the frequency equation. The modal analysis technique is used to develop the analytical solutions of the transient response. The analysis is based on an expansion of the loads, displacements in the double Fourier series that satisfy the boundary conditions. The effect of stiffener's eccentricity, number, size, and position on transient response of the shells is examined. The theoretical results are verified by comparison with FEM results.

1. INTRODUCTION

Fiber-reinforced laminated composites are extensively used in advanced structures such as pressure vessels, airplanes, submarine hulls, and missiles because of the excellent mechanical properties of these materials, such as the high specific stiffness and specific strength compared with traditional metal materials. To obtain the sufficient stiffness suitable to design requirement, we must laminate thickness thick using these composite materials. This leads to heavy structure and high cost. We need another method to get the sufficient stiffness of the thin-walled composite structures. To enhance the stiffness of these structures, we can use beam-type stiffeners. Especially, the rings in the cylindrical shell are very good stiffening elements to raise the stiffness without great mass increase.

Ring-stiffened cylindrical shells are widely used in engineering fields. These structures are subjected to external dynamic loads. These external dynamic loads can cause the undesirable resonance and it can lead to fatigue. Moreover, one must use the dynamic characteristics on design of structure because only vibration (not fatigue) could severely damage the sensitive equipment in airplanes and submarines, etc. Therefore, it is essential to understand the dynamic behavior of these structures. Theoretical methods of analyzing the stiffened structures are classified into two main types, depending upon whether the stiffeners are treated by averaging their properties over the shell surface to orthotropic materials or by considering them as discrete elements. The first method, the so-called smeared stiffener

0022-460X/02/$35.00

theory, is particularly applicable only when large numbers of stiffeners are closely and evenly spaced. The second method, the so-called discrete stiffener theory, is more general as it can accommodate any stiffener distribution.

For the ring-stiffened cylindrical shells many researchers conducted the free vibration analysis. Mustafa and Ali [1] predicted natural frequencies for the stiffened cylindrical shells using the Rayleigh–Ritz procedure. In this procedure they used only one term in assuming the displacement functions satisfying the simply supported boundary condition. One-term approximation is sufficient for the analysis of the cylindrical shells with the simply supported boundary condition. However, it can lead to much error to obtain the exact solution of stiffened shells with any other boundary conditions. Yang and Zhou [2] presented the transfer function method to analyze the ring-stiffened shell. Lee and Kim [3, 4] investigated the effect of rotation speeds and boundary conditions on the frequencies for the orthogonally stiffened composite cylindrical shells treating the materials of stiffeners as equivalent isotropic. The mentioned papers were, however, limited to the shells with the uniform dimensional and evenly spaced stiffeners. In fact, non-uniform dimensional and unevenly spaced stiffeners are used much more in structural reinforcements. Wang *et al.* [5] solved the free vibration problem for the isotropic cylindrical shells with varying ring-stiffener distribution using the extended Ritz method.

Many researchers investigated the dynamic response of stiffened structures. Srinivasan and Krishnan [6] studied the dynamic response analysis of stiffened conical shell panels using an integral equation method in the space domain. The smearing technique is used for closely spaced stiffeners. The time-domain analysis has been done using the mode superposition method. Cheng and Dade [7] presented a spline Gauss collocation method to analyze the dynamic response of stiffened plates and shells with various constraint conditions. Bicubic B splines are used as co-ordinate functions to formulate the problem based on energy principles using the technique of piecewise Gauss integration collocation. Pegg [8] presented a comparative finite element numerical study of the effect of a ring stiffener and its size and spacing on the dynamic buckling response of a cylinder. The finite element results show that the predominant harmonics and amplitudes of response are affected by the addition of, and the size and spacing of, a ring stiffener. Sinha and Mukhopadhyay [9] investigated the dynamic response of stiffened plates and shells by the finite element method employing a high-precision arbitrary-shaped triangular shell element in which stiffeners may lie in any arbitrary direction within the element. Pedron and Combescure [10] used a modal analysis method to determine the response of an infinitely long stiffened cylindrical shell of revolution to a transient lateral pressure produced by an underwater explosion and propagating in an acoustic fluid.

The dynamic analysis for the composite stiffened structures has been the subject of numerous studies. Liao and Cheng [11] investigated the dynamic stability of laminated composite stiffened or non-stiffened plates and shells due to periodic in-plane forces at boundaries using the finite element method. Mukhopadhyay and Goswami [12] studied the transient response analysis of composite stiffened panels using the finite element method. Gong and Lam [13] analyzed the transient response of a composite submersible hull subjected to underwater explosive shock. The doubly asymptotic approximation method is employed to describe the fluid–structure interactions. The fluid–structure coupled equations were solved using coupled commercial finite element and boundary element codes. Türkmen and Mea toğ lu [14] studied experimentally and numerically the dynamic response of stiffened laminated composite plates exposed to a normal blast load. ANSYS finite element software was used in their numerical procedure.

All of the above-mentioned researches for the stiffened composite structures were solved using finite element method. However, the results using theoretical method has been

relatively little reported for the transient response analysis of the ring-stiffened composite cylindrical shells. In this paper, the theoretical method is developed to investigate the effects of ring-stiffeners on vibration characteristics and transient responses for the ring-stiffened composite cylindrical shells subjected to the step pulse loading. Love's thin shell theory combined with the discrete stiffener theory to consider the ring stiffening effect is adopted to formulate the theoretical model. The Rayleigh–Ritz procedure is applied to obtain the frequency equation. The modal analysis technique is used to develop the analytical solutions of the transient analysis. The theoretical results are verified by comparing the present numerical results from commercial software ANSYS.

2. FORMULATION

Figure 1 shows the considered ring-stiffened cylindrical shell, where R, L and h are the radius, length, and thickness of the shell respectively. The displacements of the shell in the x, ϕ and z directions are denoted u, v, and w respectively. Rings stiffen the shells evenly or unevenly. The shell and ring stiffeners are laminated with a composite material. The kth ring stiffener is located at a distance x_k measured from one end of the shell and its rectangular cross-section has a depth d_r and width b_r. Stiffening techniques considered in this paper are called as concentricity, external eccentricity, or internal eccentricity depending on whether stiffeners are placed either symmetrically, outwardly, or inwardly to the shell middle surface.

The considered ring stiffeners are spaced evenly or unevenly on the shell. The stiffeners' axial positions are shown in Figure 2. The unevenly spaced stiffeners are stiffened functionally. The symbol x_k denoting the stiffener's position is a function of space ratio, S and is given as follows:

$$x_k = \frac{L}{2} \sum_{k=1}^{N_r/2} S^{k-1} \Big/ \sum_{i=1}^{N_r/2} (1 + S^i), \tag{1}$$

where N_r is the stiffener number. This function is available for the shells with even number of stiffeners. The stiffeners are located symmetrically to the axial center of the shell. As shown in this figure, the stiffeners are located near the boundary edges in the case of $S > 1$, the axial center of the shell in the case of $S < 1$, and symmetrically to the axial center of the shell in the case of $S = 1$.

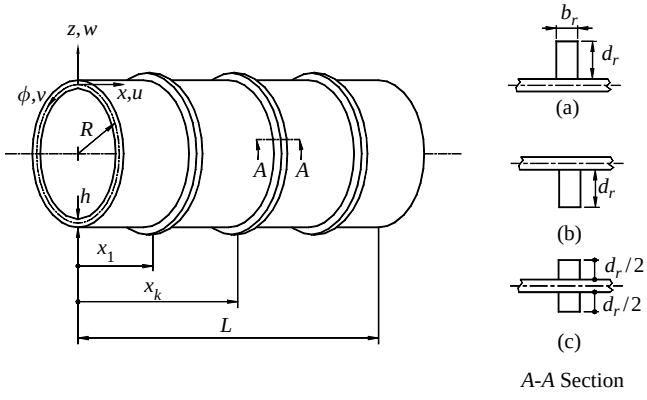

Figure 1. Co-ordinate system of ring-stiffened cylindrical shells: (a) external; (b) internal; (c) concentric.

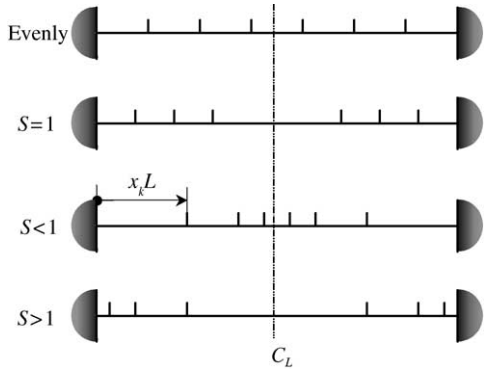

Figure 2. Ring stiffener arrangement.

The strain energy only for the symmetrically laminated, specially orthotropic and thin composite cylindrical shell [15] without the stiffeners is given by

$$U_s = \frac{1}{2}\int_0^L \int_0^{2\pi} (A_{11}\varepsilon_x^2 + 2A_{12}\varepsilon_x\varepsilon_\phi + A_{22}\varepsilon_\phi^2 + A_{66}\varepsilon_{x\phi}^2 + D_{11}\kappa_x^2 + 2D_{12}\kappa_x\kappa_\phi + D_{22}\kappa_\phi^2 + D_{66}\kappa_{x\phi}^2)\,\mathrm{d}x\,R\,\mathrm{d}\phi, \tag{2}$$

where coefficients A_{ij}, D_{ij} $(i, j = 1, 2, 6)$ are stretching and bending stiffness of composite materials and can be easily found in the literature on laminated composite structure [15]. From Love·s thin shell theory, the strain ε_i $(i = x, \phi, x\phi)$ in the middle surface and curvature κ_i $(i = x, \phi, x\phi)$ are as follows:

$$\varepsilon_x = u_{,x}, \quad \varepsilon_\phi = \frac{1}{R}(v_{,\phi} + w), \quad \varepsilon_{x\phi} = \frac{u_{,\phi}}{R} + v_{,x}, \tag{3a}$$

$$\kappa_x = -w_{,xx}, \quad \kappa_\phi = -\frac{1}{R^2}(w_{,\phi\phi} - v_{,\phi}), \quad \kappa_{x\phi} = -\frac{1}{R}(2w_{,x\phi} - v_{,x}), \tag{3b}$$

where $(,)$ is the differentiation to the space.

The deformation of the ring stiffener at distance z from the shell middle surface can be expressed as

$$u_r = u - zw_{,x}, \qquad v_r = v + \frac{z}{R}(v - w_{,\phi}), \qquad w_r = w. \tag{4}$$

The deformation of x direction for the ring stiffener, u_r, is negligible as the ring stiffener is analogous to a beam. The strain energy for a ring stiffener from the discrete stiffener theory is

$$U_k = \frac{1}{2}\int_0^{2\pi}\int_z \delta(x - x_k)[A_{22}^r\varepsilon_{\phi r}^2 + D_{22}^r\kappa_{\phi r}^2 + D_{66}^r\kappa_{x\phi r}^2](R + z)\,\mathrm{d}\phi\,\mathrm{d}z, \tag{5}$$

$$\varepsilon_{\phi r} = \frac{1}{R+z}(v_{r,\phi} + w_r), \quad \kappa_{\phi r} = -\frac{1}{(R+z)^2}(w_{r,\phi\phi} - v_{r,n}), \quad \kappa_{x\phi r} = -\frac{1}{R+z}(2w_{r,x\phi} - v_{r,x}),$$

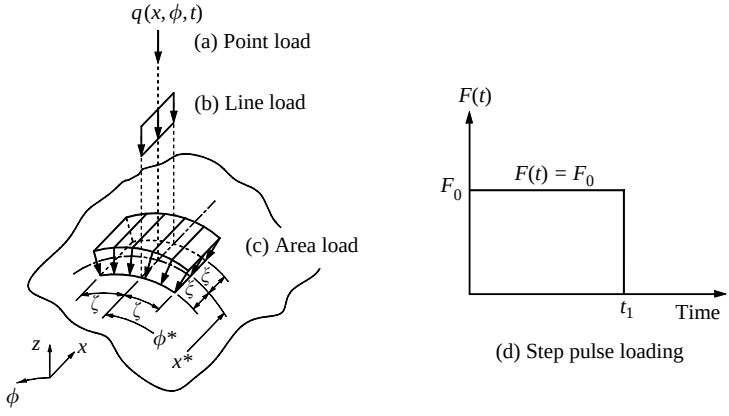

Figure 3. Applied load types and step pulse.

where superscript (or subscript) r denotes the ring stiffener and $\varepsilon_{\phi r}, \kappa_{\phi r}$ and $\kappa_{x\phi r}$ are circumferential strain, curvature and twisting curvature of the ring stiffener in the middle surface of shell respectively.

The kinetic energies of the shell and stiffener are given by

$$T_s = \frac{1}{2}\rho h \int_0^{2\pi}\int_0^{L} [\dot{u}^2 + \dot{v}^2 + \dot{w}^2]\,\mathrm{d}x R\,\mathrm{d}\phi, \tag{6}$$

$$T_k = \frac{1}{2}\rho_r b_r \int_0^{2\pi}\int_z \delta(x - x_k)[\dot{u}_r^2 + \dot{v}_r^2 + \dot{w}_r^2]\,(R + z)\,\mathrm{d}\phi\,\mathrm{d}z, \tag{7}$$

where $(\cdot)$ is the differentiation to time and ρ, ρ_r are the density.

The potential energy of the stiffened shell subjected to the transverse load $q(x, \phi, t)$ as in Figure 3 can be expressed as follows:

$$W = \int_0^{L}\int_0^{2\pi} q(x, \phi, t)\, w\,\mathrm{d}x\mathrm{R}\,\mathrm{d}\phi. \tag{8}$$

In this analysis, the beam function [4] is used as the axial mode and can be expressed in a general form as

$$\psi_m(x) = (\cosh \alpha_m x - \cos \alpha_m x) - \sigma_m(\sinh \alpha_m x - \sin \alpha_m x), \quad \alpha_m = \frac{\lambda_m}{L}, \tag{9}$$

where the coefficient σ_m is determined from the boundary condition and λ_m does not need an integer depending on the axial wave number.

The considered boundary condition is both edges clamped. The clamped condition prohibits transverse displacement and rotation. For the clamped boundary condition, the mathematical expressions using the beam function are given by

$$\psi = \psi' = 0. \tag{10}$$

The transcendental equation for λ_m and the coefficient σ_m satisfying the considered clamped–clamped boundary condition can be numerically computed from the following

formulas:

$$\cos \lambda_m \cosh \lambda_m - 1 = 0, \qquad \sigma_m = \frac{\cosh \lambda_m - \cos \lambda_m}{\sinh \lambda_m - \sin \lambda_m}. \tag{11,12}$$

The admissible displacement functions [4] for freely vibrating cylindrical shell with any boundary conditions can be written as

$$u(x, \phi, t) = \sum_{m=1}^{M} \sum_{n=0}^{N} U_{mn} \frac{\psi'_m(x)}{\alpha_m} \cos n\phi \, \eta_{mn}(t),$$

$$v(x, \phi, t) = \sum_{m=1}^{M} \sum_{n=1}^{N} V_{mn} \psi_m(x) \sin n\phi \, \eta_{mn}(t),$$

$$w(x, \phi, t) = \sum_{m=1}^{M} \sum_{n=0}^{N} W_{mn} \psi_m(x) \cos n\phi \, \eta_{mn}(t), \tag{13}$$

where U_{mn}, V_{mn}, W_{mn} are the amplitudes for each direction, m and n are axial and circumferential wave number, and ω_{mn} is the angular natural frequency for (m, n) vibration mode.

2.1. FREE VIBRATION ANALYSIS

Recognizing that at a natural frequency every point in the elastic system moves harmonically, we may assume that $\eta_{mn}(t) = \cos \omega_{mn} t$ in displacement functions. Substitute the displacement functions into each energy equation and then apply these results to the Rayleigh–Ritz procedure (14) as follows:

$$\frac{\partial}{\partial X_{mn}} \left(U_s + \sum_{k=1}^{N_r} U_k - T_s - \sum_{k=1}^{N_r} T_k - W \right) = 0, \qquad X_{mn} = [U_{mn}, V_{mn}, W_{mn}]. \tag{14}$$

As the transverse load $q(x, \phi, t)$ is not considered for the free vibration analysis, the potential energy W by the transverse loading is zero. Therefore, from the Rayleigh–Ritz procedure the following frequency equation is obtained:

$$\begin{bmatrix} K_{11} & K_{12} & K_{13} \\ K_{21} & K_{22} & K_{23} \\ K_{31} & K_{32} & K_{33} \end{bmatrix} \begin{Bmatrix} U_{mn} \\ V_{mn} \\ W_{mn} \end{Bmatrix} - \omega_{mn}^2 \begin{bmatrix} M_{11} & M_{12} & M_{13} \\ M_{21} & M_{22} & M_{23} \\ M_{31} & M_{32} & M_{33} \end{bmatrix} \begin{Bmatrix} U_{mn} \\ V_{mn} \\ W_{mn} \end{Bmatrix} = 0, \tag{15}$$

where K_{ij}, M_{ij} $(i, j = 1, 2, 3)$ are stiffness and mass matrices given in Appendix A.

Solving this eigenvalue problem the natural frequency and its corresponding mode shape are obtained. As the cylindrical shells without/with ring stiffeners have a homogeneous geometric shape for the circumferential direction, the one-term approximation is valid for the circumferential vibration mode when analyzing the vibration characteristics. Hence, the size of matrix in frequency equation (15) is $3M \times 3M$. Solving this eigenvalue problem generally gives $3M$ angular frequencies of ω_{mn}^2 for each nth circumferential mode and $3M$ corresponding eigenvectors, each containing a set of numbers for U_{mn}, V_{mn}, W_{mn}. The

eigenvalue problem is simplified as follows:

$$[\mathbf{K}][X] = \omega^2[\mathbf{M}][X], \tag{16}$$

where $[X]$ is the modal matrix consisting of eigenvectors.

2.2. TRANSIENT RESPONSE ANALYSIS

In many cases, shell structures may be subjected to dynamic loads over a limited time period rather than continuous oscillating loads. The load function in Figure 3 can be assumed as follows:

$$q(x, \phi, t) = \sum_{m=1}^{M} \sum_{n=0}^{N} F_{mn}\psi(x) \cos n\phi\, f_{mn}(t), \tag{17}$$

where coefficient F_{mn} is determined from the state of load distribution. In this study, three types of distributed loads are considered as shown in Figure 3. The following are coefficients F_{mn} for the considered load.

In the case of the unit point load acting at an arbitrary axial point (x^*, ϕ^*) of the shell, we have the following formula for coefficient F_{mn}:

$$F_{m0} = \frac{1}{\pi RL}\psi(x^*) \quad \text{for } n = 0,$$

$$F_{mn} = \frac{2}{\pi RL}\psi(x^*) \cos n\phi^* \quad \text{for } n \neq 0. \tag{18}$$

When the unit line load is uniformly distributed along a certain axial distance 2ξ at an arbitrary point of the shell, the coefficients F_{mn} are

$$F_{m0} = \frac{1}{\lambda_m R\pi}[\sinh\alpha\cosh\beta - \sin\alpha\cos\beta + \sigma_m(\sin\alpha\sin\beta - \sinh\alpha\sinh\beta)] \quad \text{for } n = 0,$$

$$F_{mn} = \frac{2}{\lambda_m R\pi}[\sinh\alpha\cosh\beta - \sin\alpha\cos\beta + \sigma_m(\sin\alpha\sin\beta - \sinh\alpha\sinh\beta)]\cos n\phi^*$$

$$\text{for } n \neq 0, \tag{19}$$

$$\alpha = \frac{\lambda_m\xi}{L}, \qquad \beta = \frac{\lambda_m x^*}{L}.$$

In the case where the unit load is uniformly distributed over a certain rectangular area $2\xi \times 2\zeta$ at an arbitrary point, the coefficients F_{mn} are

$$F_{m0} = \frac{2\zeta}{\lambda_m R\pi}[\sinh\alpha\cosh\beta - \sin\alpha\cos\beta + \sigma_m(\sin\alpha\sin\beta - \sinh\alpha\sinh\beta)] \quad \text{for } n = 0,$$

$$F_{mn} = \frac{4}{\lambda_m n\pi}[\sinh\alpha\cosh\beta - \sin\alpha\cos\beta + \sigma_m(\sin\alpha\sin\beta - \sinh\alpha\sinh\beta)]\sin\frac{n\zeta}{R}\cos n\phi^*$$

$$\text{for } n \neq 0. \tag{20}$$

It is considered in this paper that the distributed loads are applied symmetrically at the center of the shell.

The temporal portion of $f_{mn}(t)$ in equation (17) can be a harmonic loading. For this time loading it is convenient to express $f_{mn}(t)$ as the convolution integral:

$$f_{mn}(t) = \int_0^t F(\tau) \sin \omega_{mn}(t - \tau)\, \mathrm{d}\tau, \tag{21}$$

where $F(\tau)$ is the actual applied load, ω_{mn} is the angular natural frequency for the (m, n) vibration mode, and τ is a dummy time variable.

The time pulse loading considered in this paper is stepped pulse as shown in Figure 3. For the stepped pulse the force function $F(t)$ and the convolution integral $f_{mn}(t)$ are given by

$$F(t) = \begin{cases} F_0, & 0 \leqslant t < t_1, \\ 0, & t > t_1, \end{cases} \tag{22}$$

$$f_{mn} = \frac{F_0}{\omega_{mn}} \begin{cases} 1 - \cos \omega_{mn} t, & 0 \leqslant t \leqslant t_1, \\ \cos \omega_{mn}(t - t_1) - \cos \omega_{mn} t, & t > t_1, \end{cases} \tag{23}$$

where F_0 is the maximum amplitude of load.

When external loads act on the shell, the temporal portion of $\eta_{mn}(t)$ in displacement functions is not assumed unlike the vibration analysis. Substituting displacement functions (13) and force function (17) into Rayleigh–Ritz procedure (14), and applying Hamilton·s principle to the results, the equations of motion are yielded as follows:

$$[\mathbf{M}][X]\ddot{\eta}_{mn}(t) + [\mathbf{K}][X]\eta_{mn}(t) = [Q] f_{mn}(t), \tag{24}$$

where matrix $[Q]$ consists of (1×3) sub-matrix with dimension $(M \times M)$ given in Appendix A. These equations of motion are a set of $3M$-coupled ordinary differential equations of second order. The solution of these equations becomes more complex when the degree of freedom of system is large and/or when the load functions are not periodic. In such cases, we can obtain a set of $3M$-uncoupled differential equations of second order using the modal analysis technique as in the following procedures.

Multiplying equation (24) by $[X]^{\mathrm{T}}$ we obtain

$$[X]^{\mathrm{T}}[\mathbf{M}][X]\ddot{\eta}_{mn}(t) + [X]^{\mathrm{T}}[\mathbf{K}][X]\eta_{mn}(t) = [X]^{\mathrm{T}}[Q] f_{mn}(t). \tag{25}$$

Normalizing the normal modes, we have

$$[X]^{\mathrm{T}}[\mathbf{M}][X] = [I], \qquad [X]^{\mathrm{T}}[\mathbf{K}][X] = \omega_{mn}^2 [I]. \tag{26a, b}$$

Equation (25) can be expressed, using equations (25a, b), as

$$[I]\ddot{\eta}_{mn}(t) + \omega_{mn}^2 [I]\eta_{mn}(t) = [P] f_{mn}(t), \qquad [P] = [X]^{\mathrm{T}}[Q]. \tag{27}$$

Equation (27) denotes a set of $3M$-uncoupled differential equation of second order. The solution of these equations can be expressed using convolution integral as follows:

$$\eta_{mn}(t) = \frac{P_{mn}}{\omega_{mn}} f_{mn}(t) = \frac{P_{mn}}{\omega_{mn}} \int_0^t F(\tau) \sin \omega_{mn}(t - \tau)\, \mathrm{d}\tau. \tag{28}$$

Substituting equation (28) into lateral displacement function, $w(x, \phi, t)$, we obtain the lateral displacement function of ring-stiffened composite cylindrical shells subjected to external pulse loads.

$$w(x, \phi, t) = \sum_{m=1}^{M} \sum_{n=0}^{N} \frac{W_{mn} P_{mn}}{\omega_{mn}} \sin \frac{m\pi x}{L} \cos n\phi \int_0^t F(\tau) \sin \omega_{mn}(t - \tau) \, d\tau. \tag{29}$$

3. RESULTS AND DISCUSSIONS

Some numerical examples are now demonstrated for the present theoretical method. The used graphite/epoxy (T300/NY556/HY917) composite material and basic geometric properties are given in Table 1.

Comparisons are made with finite element method to check the validity of the present theoretical method. ANSYS commercial FEM code [16] is used for the finite element analysis procedures. The element used in FEA is the multi-layered shell element, SHELL99, which has eight-nodes and six-degrees of freedom per node. In the FE model, a half model for the vibration analysis is considered because the circumferential vibration modes are symmetric to any radial axis and a quarter model for the transient response analysis because the responses are symmetric to the axial and circumferential direction if the load applies to the center of the cylindrical shell. The eigenvalue problem formulated within the FEM for the vibration analysis is solved by the reduced subspace analysis method included in the ANSYS code. The full analysis method is used for the transient response problem to be applicable to the structures subjected to the element load.

In Table 2, the convergence studies are conducted for the first five lower frequencies of the unstiffened and stiffened composite cylindrical shells. Also, the converged frequencies and the corresponding mode shapes are compared with the results from the finite element analysis. The composite cylindrical shells with shell's length-to-radius ratio, $L/R = 2{\cdot}5$ are stiffened evenly or unevenly by four-internally eccentric ring stiffeners with stiffener's depth-to-width ratio, $d_r/b_r = 3$. There are some differences in results between the one-term and multi-term approximation methods. The maximum difference is about 5% for unstiffened shell, 6% for the shells with evenly and unevenly spaced ($S = 0{\cdot}5$) stiffeners, and 8% for the shell with unevenly spaced stiffeners ($S = 2{\cdot}0$). Also, for the shell with unevenly spaced stiffeners there is slight difference of mode sequences. This means that the one-term approximation method is not appropriate to predict the natural frequency and mode shape. It is obvious that the multi-term approximation method must be adopted to obtain reasonable results for the Rayleigh–Ritz procedure. There is a good agreement between FEM results and the converged values of the theoretical method, thus validating the present

TABLE 1

Material and geometric properties of the composite cylindrical shell

Material properties		Geometric properties	
E_1	139·4 GPa	Shell radius	200 mm
E_2	8·7 GPa	Shell thickness	2 mm
G_{12}	3·1 GPa	Thickness of each layer	0·125 mm
v_{12}	0·268	Stiffener width	2 mm
ρ	1542 kg/m^3	Stacking sequence	$[(\pm 45^\circ/0^\circ/90^\circ)_2]_S$

TABLE 2

Convergence and comparison study with FEM results of natural frequencies for the unstiffened/stiffened cylindrical shells ($R = 0{\cdot}2$ m, $L/R = 2{\cdot}5$, $d_r = 3b_r$, $N_r = 4$)

Natural frequency (Hz)					
$M = 1$	$M = 6$	$M = 10$	$M = 12$	$M = 14$	FEM
(a) *Unstiffened shell*					
617·15 (1,6)	601·10 (1,5)	597·03 (1,5)	596·13 (1,5)	595·57 (1,5)	587·23 (1,5)
617·21 (1,5)	607·61 (1,6)	605·20 (1,6)	604·69 (1,6)	604·38 (1,6)	594·13 (1,6)
712·27 (1,7)	706·13 (1,7)	704·59 (1,7)	704·26 (1,7)	704·09 (1,7)	691·71 (1,7)
746·83 (1,4)	719·40 (1,4)	712·48 (1,4)	710·89 (1,4)	709·85 (1,4)	701·68 (1,4)
869·37 (1,8)	864·67 (1,8)	863·53 (1,8)	863·29 (1,8)	863·15 (1,8)	848·47 (1,8)
(b) *Internally stiffened shell*: *evenly spaced*					
808·00 (1,4)	784·13 (1,4)	776·16 (1,4)	773·94 (1,4)	773·04 (1,4)	750·50 (1,4)
835·47 (1,5)	824·31 (1,5)	815·90 (1,5)	814·15 (1,5)	813·75 (1,5)	777·35 (1,5)
1026·8 (1,3)	981·67 (1,3)	970·09 (1,3)	966·99 (1,3)	965·14 (1,3)	943·33 (1,3)
1043·4 (1,6)	1038·4 (1,6)	1022·4 (1,6)	1019·8 (1,6)	1019·7 (1,6)	962·03 (1,6)
1344·4 (2,5)	1322·4 (2,5)	1309·3 (2,5)	1307·6 (2,5)	1306·4 (2,5)	1233·0 (2,5)
(c) *Internally stiffened shell*: *unevenly spaced with* $S = 0{\cdot}5$					
825·14 (1,4)	800·58 (1,4)	794·43 (1,4)	792·39 (1,4)	789·48 (1,4)	764·50 (1,4)
890·61 (1,5)	874·03 (1,5)	870·36 (1,5)	868·99 (1,5)	863·79 (1,5)	822·56 (1,5)
1021·9 (1,3)	997·63 (1,3)	966·43 (1,3)	963·42 (1,3)	961·27 (1,3)	938·94 (1,3)
1141·0 (1,6)	1118·8 (1,6)	1115·0 (1,6)	1113·8 (1,6)	1103·3 (1,6)	1039·8 (1,6)
1354·1 (2,5)	1317·4 (2,5)	1309·0 (2,5)	1305·0 (2,5)	1303·0 (2,5)	1233·3 (2,5)
(d) *Internally stiffened shell*: *unevenly spaced with* $S = 2{\cdot}0$					
669·73 (1,5)	659·49 (1,5)	655·87 (1,5)	655·09 (1,5)	654·33 (1,5)	638·91 (1,5)
728·79 (1,6)	709·77 (1,6)	706·80 (1,6)	706·17 (1,6)	705·35 (1,6)	685·63 (1,6)
760·53 (1,4)	736·27 (1,4)	730·09 (1,4)	728·48 (1,4)	727·31 (1,4)	714·30 (1,4)
890·63 (1,7)	826·19 (1,7)	822·53 (1,7)	821·63 (1,7)	820·55 (1,7)	798·38 (1,7)
1038·1 (1,3)	980·59 (1,8)	975·39 (1,8)	974·43 (1,8)	973·37 (1,8)	949·39 (1,8)

Numbers in (m, n) represent the axial and circumferential wave numbers.

theoretical method. The frequencies from the theoretical method are somewhat higher than those from the finite element method. This is the reason why the theoretical results generally provide the upper bounds. It may be observed that using $M = 14$ for each displacement function in multi-term approximation is adequate for converged results of all considered shells in vibration analysis.

Figure 4 indicates the convergence of the lateral deflections at the center of the unstiffened/stiffened shells considered in Table 2. The shells are subjected to point step pulse load at the center of shell: the load is applied with the amplitude, $F_0 = 1{\cdot}0$ kN during 1·5 ms. As shown in this figure, the deflections in small series number are much smaller than those in large series number for all considered shells. Therefore, we must use a large enough series number to obtain reasonable results. For the transient analysis the use of (30, 50) series number is adequate for the converged results.

Figure 5 shows the comparison of the transient response between the theoretical and finite element methods for the model considered in Figure 4. The results from the two methods agree well. As indicated in this figure, the results from FEM are somewhat higher than those from the theoretical method. This is because the lateral deflection is inversely

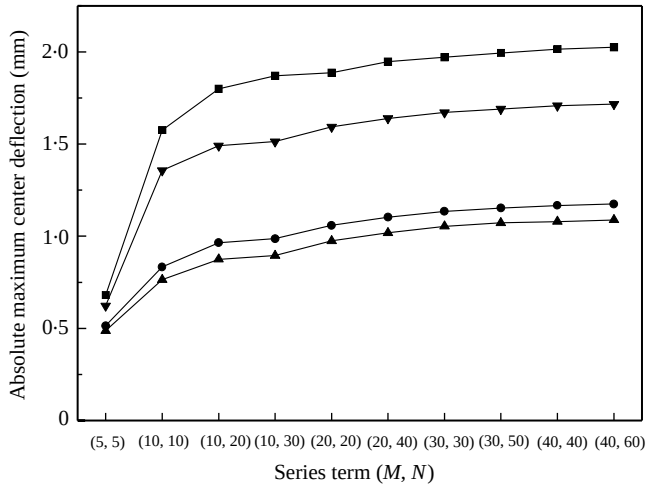

Figure 4. Convergence study for unstiffened/stiffened shells subjected to point step pulse loading in Table 2 ($L/R = 2{\cdot}5$, $d_r = 3b_r$, $F_0 = 1{\cdot}0$ kN, $t_1 = 1{\cdot}5$ ms): —■—, unstiffened; —●—, evenly spaced; —▲—, unevenly spaced with $S = 0{\cdot}5$; —▼—, unevenly spaced with $S = 2{\cdot}0$.

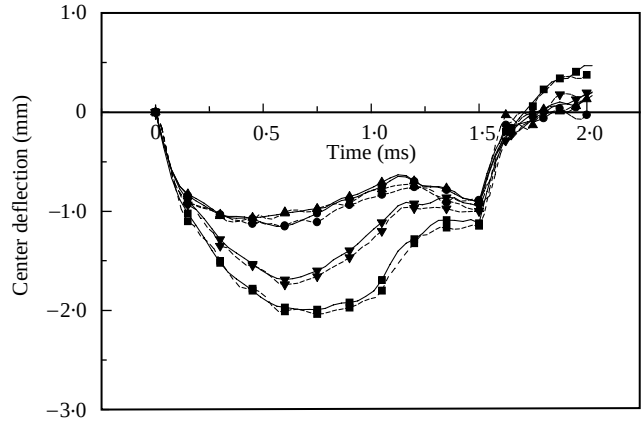

Figure 5. Comparison of center deflection with FEM for the unstiffened/stiffened shells in Figure 4: - - - - - - -, FEM; ——, theory; ■, unstiffened; ●, evenly spaced; ▲, unevenly spaced with $S = 0{\cdot}5$; ▼, unevenly spaced with $S = 2{\cdot}0$.

proportion to the angular frequency as indicated in equation (29): the frequency from the theoretical method is higher than that from the finite element method as presented in Table 2.

Figure 6 shows the effect of concentricity and eccentricity of stiffeners for the six-evenly spaced ring-stiffened composite cylindrical shells with $L/R = 2$. The stiffener's aspect ratio, d_r/b_r is 5. The point step pulse loading is applied with 1·0 kN amplitude at the center of shell during $t_1 = 1{\cdot}0$ ms. The fundamental frequency (f_1) of shells with eccentric stiffeners is much higher than that of shells with concentric stiffeners. For the eccentrically stiffened shell, the frequency of the shell with the internal stiffeners is higher than that of the shell with the external stiffeners. From this result, we can estimate that the internally stiffened shell with the highest frequency has the smallest deflection. Like the estimation the deflection of the internally stiffened shell is the smallest and that of the concentrically stiffened shell is the

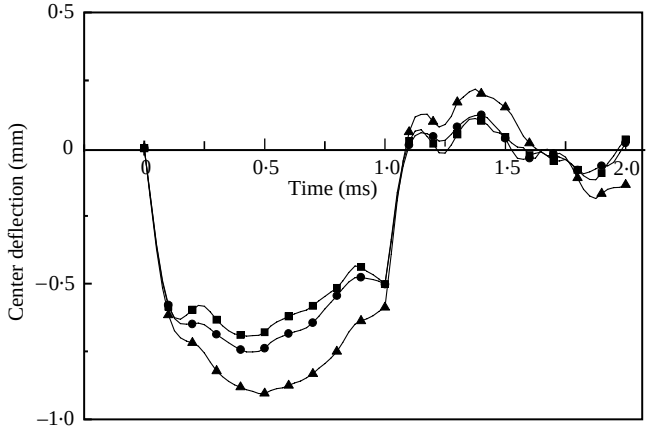

Figure 6. Effect of stiffener eccentricity on center deflection for the six evenly spaced ring-stiffened shells subjected to point step pulse loading ($L/R = 2$, $d_r = 5b_r$, $F_0 = 1{\cdot}0$ kN, $t_1 = 1{\cdot}0$ ms): —■—, internal: $f_1 = 988{\cdot}6$ Hz; —●—, external: $f_1 = 40{\cdot}2$ Hz; —▲—, concentric: $f_1 = 809{\cdot}0$ Hz.

largest. It is notable that eccentric stiffeners are more effective than concentric ones and internally eccentric stiffeners are more efficient than externally eccentric stiffeners in raising the fundamental frequency or decreasing the deflection.

Figure 7 indicates the effect of ring stiffener location on dynamic characteristics for the internally stiffened cylindrical shell with $L/R = 4$, $d_r/b_r = 4$ subjected to the step point or line pulse loading. The maximum amplitude of loads, F_0 for the point loading is 1·0 kN acting on the center of the shell and for the line loading 5 kN/m on $2\xi = 0{\cdot}5L$ of the shell during $t_1 = 1{\cdot}0$ ms. The dashed lines denote the results for the evenly spaced shell. The frequency of the shells where the rings are positioned near the center of the shells (in the case of $S < 1$) is much higher than that of the shells where the rings are positioned near the two edges of the shells ($S > 1$). That is, as the stiffeners are positioned near the center of shells ($S < 1$), the frequencies of the shells increase and become larger than those of the evenly spaced shell. However, as the stiffeners are positioned near the edges ($S > 1$), the frequencies decrease and become smaller than those of the evenly spaced shell. The deflection of the shell with $S < 1$ is slightly smaller or larger than that of evenly spaced shell. In the case of $S > 1$, the deflection increases rapidly with space ratio, S. This is because the positioning of the stiffeners near axial center increases the stiffness of the shell. This result shows that dynamic characteristics may be influenced by the stiffener positions. Designers may obtain the desirable dynamic characteristics adequate to design purpose as they arrange the stiffeners appropriately.

Figure 8 illustrates the effect of eccentricity (or stiffener's aspect ratio, d_r/b_r) on the fundamental frequency and the maximum center deflection for the various stiffened shells. The shells with $L/R = 2$ are subjected to point step pulse loading of 1·0 kN during 1·0 ms. Figure 8(a) indicates the increase percentage of fundamental frequency and Figure 8(b) indicates the decrease percentage of maximum deflection calculated by the following equations:

$$\text{Increase percentage of fundamental frequency (\%)} = \frac{f_u - f_s}{f_u} \times 100,$$

$$\text{Decrease percentage of maximum deflection (\%)} = \frac{\delta_u - \delta_s}{\delta_u} \times 100,$$

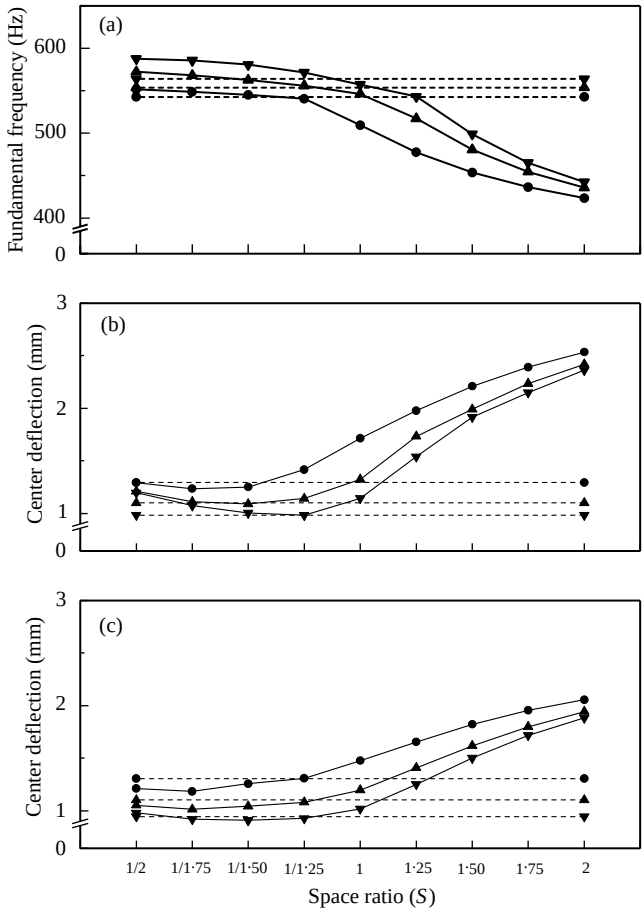

Figure 7. Effect of stiffener position for the internally eccentric ring-stiffened shells subjected to point and line step pulse loading ($L/R = 3$, $d_r/b_r = 5$, $t_1 = 1{\cdot}0$ ms): —●—, $N_r = 4$; —▲—, $N_r = 6$; —▼—, $N_r = 8$. (a) frequency variation; (b) line load: $F_0 = 5{\cdot}0$ kN/m; (c) point load: $F_0 = 1{\cdot}0$ kN.

where f_u, f_s are the fundamental frequencies and δ_u, δ_s the maximum deflections of the unstiffened/stiffened shell. It is seen from the figure that as the eccentricity increases, the frequency increases nearly proportionally while the frequency decreases inversely in the extreme case of the shell stiffened by many rings with the large eccentricity. For the shell with extreme eccentricity, $d_r/b_r = 13$, the frequencies decrease by adding more rings. Each ring imposes not only stiffness but also mass loading effect on the shell. Thus, this phenomenon occurred because mass loading effects activate greater than stiffness effects on the fundamental frequency of the shells with excessive ring eccentricity. The deflection decreases exponentially at the first small eccentricity but above any d_r/b_r ratio (about 9) the deflection remains almost the same. The maximum deflection of the shell with $d_r/b_r = 1$ decreases only about 3–10% compared with that of unstiffened shell. However, that of the shell with $d_r/b_r = 2$ decreases about 11–40%. From this, one should stiffen the shell with the ring of $d_r/b_r = 2$–9 to obtain an efficient stiffening effect. This result indicates that the eccentricity of stiffener can significantly influence vibration characteristics and transient response. The excessive eccentricity is not good at structural characteristics because the ring stiffening effect is very small and the stiffened structure is to be buckled locally on slender stiffeners.

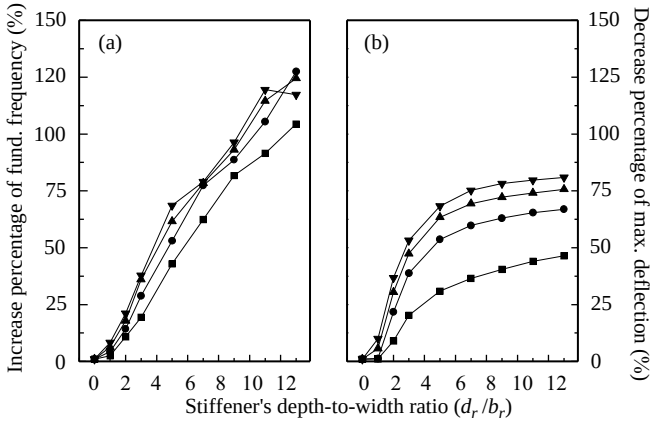

Figure 8. Effect of stiffener's depth-to-width ratio for the evenly spaced, internally eccentric ring-stiffened cylindrical shells subjected to point step pulse loading ($L/R = 2$, $F_0 = 1{\cdot}0$ kN, $t_1 = 1{\cdot}0$ ms): —■—, $N_r = 1$; —●—, $N_r = 3$; —▲—, $N_r = 5$; —▼—, $N_r = 7$.

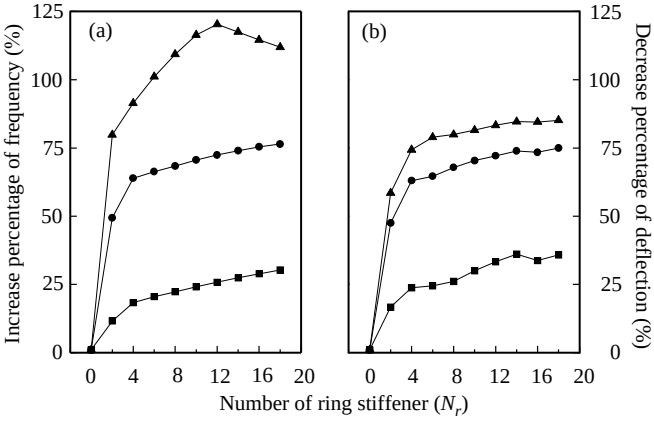

Figure 9. Effect of stiffener number for the evenly spaced, internally eccentric ring-stiffened shells subjected to area step pulse loading ($L/R = 3$, $d_r/b_r = 5$, $F_0 = 200$ kN/m^2, $t_1 = 1{\cdot}0$ ms): —■—, $d_r/b_r = 2$; —●—, $d_r/b_r = 5$; —▲—, $d_r/b_r = 8$.

Figure 9 is given to investigate the effect of stiffener number for the evenly spaced, internally eccentric stiffened shells. The shells with $L/R = 3$ are subjected to the area step pulse loading with 200 kN/m^2 during $t_1 = 1{\cdot}0$ ms. The loading area (A_o) is $0{\cdot}3L \times 0{\cdot}1H$, where H is the circumferential arc length. It is noted that the stiffening effect is not great although many stiffeners with small d_r/b_r ratio add to the shell but magnificent in the case that the shells are stiffened by stiffeners with relatively large d_r/b_r ratio. For example, adding the only two ring stiffeners with $d_r/b_r = 8$ on the shell the fundamental frequency increases about 80% and the center deflection reduces about 60% compared with the unstiffened shell. However, for the corresponding shell with $d_r/b_r = 2$ the frequency rises about 10% and the deflection decreases about 20%. The maximum value increasing the frequency or reducing the deflection by adding the stiffeners with $d_r/b_r = 2$ on the shells is only about 30% in the considered case. For small stiffener numbers the maximum center deflections decrease dramatically with the increase of stiffener number. However, as stiffeners are more added to the shell the change of the frequency or deflection nearly does not occur. In the

extreme case the frequency decreases conversely. This figure shows that although it is advantageous to have few stiffeners to increase the fundamental frequency or to decrease the deflection, many stiffeners do not necessarily lead to proportional increase of fundamental frequency or decrease of deflection. Therefore, few stiffeners are adequate to raise the frequency or to reduce the deflection.

4. CONCLUSIONS

In this paper, the theoretical method is developed to investigate the effects of ring stiffeners on vibration characteristics and transient response for the ring-stiffened composite cylindrical shells subjected to the step pulse loading. As there are no published results available on the transient response of the ring-stiffened composite cylindrical shells, the present theoretical results are verified by comparing the present finite element results from ANSYS. Based on the numerical results, the following are concluded.

The eccentric stiffening is more effective than the concentric to increase frequency or decrease the deflection. The appropriate stiffener's eccentricity (or depth-to-width ratio) leads to an increase in the frequency and a decrease in the deflection, but the excessive eccentricity decreases the frequency on the contrary and does not decrease the deflection. Few stiffeners are adequate to raise the frequency or to reduce the deflection. Adding the ring greatly decreases the frequency but does not decrease the deflection. The proper arrangement of ring-stiffeners may result in the desirable effect of raising the frequency or decreasing the deflection.

ACKNOWLEDGMENTS

This work was supported by Korean Research Foundation Grant (KRF-2000-E00006).

REFERENCES

1. B. A. J. MUSTAFA and R. ALI 1989 *Computers and Structures* **32**, 355–363. An energy method for free vibration analysis of stiffened circular cylindrical shells.
2. B. YANG and J. ZHOU 1995 *Journal of Applied Mechanics* **62**, 1005–1014. Analysis of ring–stiffened cylindrical shells.
3. Y. S. LEE and Y. W. KIM 1998 *Computers and Structures* **69**, 271–281. Vibration analysis of rotating composite cylindrical shells with orthogonal stiffeners.
4. Y. S. LEE and Y. W. KIM 1999 *Advanced in Engineering Software* **30**, 649–655. Effect of boundary conditions on natural frequencies for rotating composite cylindrical shells with orthogonal stiffeners.
5. M. WANG, S. SWADDIWUDHIPONG and J. TIAN 1997 *Journal of Engineering Mechanics* **123**, 134–142. Ritz method for vibration analysis of cylindrical shells with ring stiffeners.
6. R. S. SRINIVASAN and P. A. KRISHNAN 1989 *Computers and Structures* **33**, 831–837. Dynamic analysis of stiffened conical shell panels.
7. S. P. CHENG and C. DADE 1990 *Computers and Structures* **36**, 623–629. Dynamic analysis of stiffened plates and shells using spline Gauss collocation method.
8. N. G. PEGG 1992 *Computers and Structures* **44**, 1205–1214. A numerical study of dynamic pulse buckling of ring-stiffened cylinders.
9. G. SINHA and M. MUKHOPADHYAY 1995 *Journal of Vibration and Acoustics, Transactions of American Society of Mechanical Engineers* **117**, 11–16. Transient dynamic response of arbitrary stiffened shells by the finite element method.
10. C. PEDRON and A. COMBESCURE 1995 *Thin-Walled Structures* **23**, 85–105. Dynamic buckling of stiffened cylindrical shells of revolution under a transient lateral pressure shock wave.

11. C. L. LIAO and C. R. CHENG 1994 *Journal of Sound and Vibration* **174**, 335–351. Dynamic stability of stiffened laminated composite plates and shells subjected to in-plane pulsating forces.
12. M. MUKHOPADHYAY and S. GOSWAMI 1996 *Aeronautical Journal* **100**, 223–233. Transient finite element dynamic response of laminated composite stiffened shell.
13. S. W. GONG and K. Y. LAM 1998 *Composite Structures* **41**, 27–37. Transient response of stiffened composite submersible hull subjected to underwater explosive shock.
14. H. S. TÜRKMEN and Z. MEO TOĞ LU 1999 *Journal of Sound and Vibration* **221**, 371–389. Dynamic response of a stiffened laminated composite plate subjected to blast load.
15. J. R. VINSON 1993 *The Behavior of Shells Composed of Isotropic and Composite Materials*. Dordrecht: Kluwer Academic Publishers.
16. SASI 2000 *ANSYS User's Manual*. Houston: Swanson Analysis System Inc.

APPENDIX A

The coefficients of K_{ij}, M_{ij} in equation (15) are as follows:

$$K_{11} = \frac{R\pi}{2}\left(A_{11}\frac{X^{22}}{\alpha_i\alpha_m} + \frac{n^2A_{33}}{R^2}\frac{X^{11}}{\alpha_i\alpha_m}\right), \tag{A1}$$

$$K_{12} = \frac{Rn\pi}{2}\left(\frac{A_{12}}{R}\frac{X^{02}}{\alpha_i} - \frac{A_{33}}{R}\frac{X^{11}}{\alpha_i}\right), \tag{A2}$$

$$K_{13} = \frac{Rn\pi}{2}\frac{A_{12}}{R}\frac{X^{02}}{\alpha_i}, \tag{A3}$$

$$K_{22} = \frac{R\pi}{2}\left[n^2\left(A_{22} + \frac{D_{22}}{R^2}\right) + A_{33} + \frac{D_{33}}{R^2}\right]\frac{X^{22}}{R^2} + \sum_{k=1}^{N_r}\frac{\pi}{2}\left[\left(\frac{d_r}{R} + \frac{S_r}{R^2}\right)(n^2A^r_{22}\boldsymbol{\Psi}^{00} + D^r_{66}\boldsymbol{\Psi}^{11}) + \left(\frac{d_r}{R^3} - \frac{S_r}{R^4}\right)n^2D^r_{22}\boldsymbol{\Psi}^{00}\right], \tag{A4}$$

$$K_{23} = \frac{Rn\pi}{2}\left[\left(A_{22} + \frac{n^2D_{22}}{R^2}\right)\frac{X^{00}}{R^2} + \frac{D_{12}}{R^2}X^{02} + 2D_{22}X^{11}\right] + \sum_{k=1}^{N_r}\frac{\pi}{2R^2}\left[nA^r_{22}(n^2S_r + d_rR)\boldsymbol{\Psi}^{00} + n^3D^r_{22}\left(\frac{d_r}{R} - \frac{S_r}{R^2}\right)\boldsymbol{\Psi}^{00} + D^r_{66}(4d_rR - I_r)\boldsymbol{\Psi}^{11}\right], \tag{A5}$$

$$K_{33} = \frac{R\pi}{2}\left[\left(A_{22} + \frac{n^4D_{22}}{R^2}\right)\frac{X^{00}}{R^2} + D_{11}X^{22} - 2\frac{n^2D_{12}}{R^2}(X^{02} + X^{20}) + 4\frac{n^2}{R^2}D^{66}X^{11}\right] + \sum_{k=1}^{N_r}\frac{\pi}{2}\left[A^r_{22}\left\{\frac{d_r}{R} + \frac{S_r}{R^2}(2n^2 - 1) + \frac{n^2I_r}{R^2}(n^2 - 2) - \frac{n^4I'_r}{R^4}\right\}\boldsymbol{\Psi}^{00} + n^4D^r_{22}\left(\frac{d_r}{R^3} - \frac{S_r}{R^4}\right)\boldsymbol{\Psi}^{11} + D^r_{66}\left(\frac{4d_r}{R} - \frac{3I_r}{R^3} - \frac{I'_r}{R^4}\right)\boldsymbol{\Psi}^{11}\right], \tag{A6}$$

$$M_{11} = \frac{\rho hR\pi}{2}\frac{X^{11}}{\alpha_i\alpha_m} + \sum_{k=1}^{N_r}\frac{\rho_rb_r\pi}{2}(d_rR + S_r)\frac{\boldsymbol{\Psi}^{11}}{\alpha_i\alpha_m}, \tag{A7}$$

$$M_{13} = -\sum_{k=1}^{N_r}\frac{\rho_rb_r\pi}{2}(S_rR + I_r)\frac{\boldsymbol{\Psi}^{11}}{\alpha_i}, \tag{A8}$$

$$M_{22} = \frac{\rho h R \pi}{2} X^{00} + \sum_{k=1}^{N_r} \frac{\rho_r b_r \pi}{2} (d_r R^3 + 3 S_r R^2 + 3 I_r R + I'_r) \boldsymbol{\Psi}^{00}, \tag{A9}$$

$$M_{23} = \sum_{k=1}^{N_r} \frac{\rho_r b_r n \pi}{2} (S_r R^2 + 2 I_r R + I'_r) \boldsymbol{\Psi}^{00}, \tag{A10}$$

$$M_{33} = \frac{\rho h R \pi}{2} X^{00} + \sum_{k=1}^{N_r} \frac{\rho_r b_r \pi}{2} \left[\left\{ \frac{n^2}{R^2} (I_r R + I'_r) + d_r R + S_r \right\} \boldsymbol{\Psi}^{00} + (I_r R + I'_r) \boldsymbol{\Psi}^{11} \right], \tag{A11}$$

$$K_{31} = K_{13}, \quad K_{32} = K_{23}, \quad M_{32} = M_{23}, \tag{A12}$$

where

$$X^{pq} = \int_0^L \frac{\partial^{(p)} \psi_i}{\partial x^{(p)}} \frac{\partial^{(q)} \psi_m}{\partial x^{(q)}} \mathrm{d}x, \tag{A13}$$

$$\boldsymbol{\Psi}^{pq} = \int \delta(x - x_k) \frac{\partial^{(p)} \psi_i}{\partial x^{(p)}} \frac{\partial^{(q)} \psi_m}{\partial x^{(q)}} \mathrm{d}x, \tag{A14}$$

$$\begin{Bmatrix} S_r \\ I_r \\ I'_r \end{Bmatrix} = \int \begin{Bmatrix} z \\ z^2 \\ z^3 \end{Bmatrix} \mathrm{d}z. \tag{A15}$$

The coefficients of Q_i in equation (24) are as follows:

$$Q_1 = Q_2 = 0, \qquad Q_3 = \frac{R\pi}{2} f_{mn} X^{00}. \tag{A16, A17}$$